Wear 523 (2023) 204864

Contents lists available at ScienceDirect

Wear

journal homepage: www.elsevier.com/locate/wear

Dynamic pressure scuffing initiation of a grade 250 flake graphite cast iron

J.C. Walker [a,*], H.G. Jones [b], T.J. Kamps [b]

[a] National Centre for Advanced Tribology (nCATS), University of Southampton, UK
[b] National Physical Laboratory, Teddington, UK

ARTICLE INFO

Keywords:
Scuffing
Cast iron
Contact pressure
Oxidational wear

ABSTRACT

The dynamic contact pressures experienced at the ring-liner interface of an engine are difficult to replicate in laboratory based reciprocating tribometers utilising a sliding Hertzian line contact, not least due to wear of the mating surfaces. A grade 250 flake graphite cast iron flat plate test geometry was designed to allow dynamic contact pressures between 8 and 62 MPa experienced in a heavy-duty diesel engine liner to be achieved on a reciprocating tribometer during the compression and expansion stroke.A constant normal load of 311 N was applied by sliding at 25 mm stroke length in PAO4 at 15 Hz against a 52100 rectangular contact area (2 × 20 mm). The temperature was slowly increased at 4 °C/min to initiate scuffing between the mating surfaces. Severe scuffing initiated at 250.8 ± 2.6 °C for all specimens. The spatially resolved friction force and non-contact optical profilometry suggested scuffing did not always initiate in the region of the highest contact pressure, whilst electron microscopy revealed that subsequent to lubricant failure, a transient low friction iron oxide layer was formed prior to removal and catastrophic adhesive wear.

1. Introduction

The use of low viscosity lubricants for off-grid heavy duty diesel engines is an effective approach to improve emissions and fuel efficiency by reducing friction generated by viscous shear [1,2]. However thinner lubricating films between reciprocating sliding contacts can increase the propensity of asperity contact under transient loading conditions that exceed the normal operating envelope. Frictional heat dissipation under such circumstances necessarily further thins the lubricant, such that a cumulative damage process known as scuffing can initiate [3–6]. Scuffing has a number of broad definitions [6–8] across multiple categories of wear mechanisms indicating its complex and multi-variable nature which at times can appear stochastic. In extreme conditions, this leads to catastrophic engine damage and seizure of reciprocating components. The initiation of scuffing is often subtle whilst progression to final failure exhibits a rapid rise in the average coefficient of friction (0.04 s^{-1}) [9,10]. Attempts to identify the complex variables that contribute to the initiation stage range from acoustic emission [11,12] and electrostatic [13] detection techniques, *in situ* optical, interferometric and XRD [14–16], as well as signal processing of friction force measurements [17–19]. Kamps et al. [17,18] developed a ramped load scuffing criteria based on deviations of the friction force at the stroke reversal positions, where scuffing initiation was expected to take place, when compared to the root mean squared (rms) friction of the entire stroke. They were able to interrupt sliding of grade 250 cast iron surfaces during the mild initiation phase in order to correlate surface cracking at the pearlitic-graphitic interface, similar to a plastic fatigue mechanism proposed by Ludema [8], to subsequent adhesive transfer to the counter surface during the severe scuffing stage. This paper builds on this approach by deploying the same methodology for scuffing on a variable geometry dynamic pressure specimen. Walker et al. [20] have recently shown that the contact pressures experienced by the top compression ring of a heavy duty diesel engine can be dynamically replicated on a laboratory scale bench top reciprocating tribometer by matching the geometry of the test surface to the profile of crank angle resolved force. The dependence of scuffing on temperature was reinforced, yet formation of oxide-induced tribo-film formation was influenced by contact pressure in the boundary condition subsequent to lubricant desorption. The present paper utilises the rms friction methodology to determine scuffing initiation of variable geometry dynamic pressure surfaces and correlate specific surface tribo-film species formation to the onset of severe scuffing.

* Corresponding author.
E-mail address: j.walker@soton.ac.uk (J.C. Walker).

https://doi.org/10.1016/j.wear.2023.204864
Received 3 October 2022; Received in revised form 14 January 2023; Accepted 1 February 2023
Available online 29 March 2023
0043-1648/© 2023 The Authors. Published by Elsevier B.V. This is an open access article under the CC BY license (http://creativecommons.org/licenses/by/4.0/).

2. Methodology

2.1. Specimen manufacture

A Phoenix Tribology TE77 high frequency reciprocating tribometer was used to replicate the variable contact pressures experienced by the top compression ring of a 12.8-L heavy duty diesel engine during scuffing. Rectangular test coupons of dimensions 58 × 38 × 4 mm were machined from a grade 250 cast iron billet supplied by West Yorkshire Steel Ltd (UK). The test surface was ground at 45° to the length dimension to represent a honed cylinder liner surface. To create a dynamic pressure variable geometry specimen, the normal load profile of the top compression ring from a 12.8 L heavy duty diesel during the expansion stroke, Fig. 1, was utilised to machine a 1 mm recess in the test surface such that a symmetrical profile parallel to the sliding direction would facilitate a similar dynamic contact pressure, Fig. 2.

Peak contact pressures of the top compression ring in large diesel engines have been found to be as high as 70 MPa [21], while mean pressures during the intake and exhaust strokes are closer to 8 MPa [20]. The distance between the symmetrical profiles perpendicular to the sliding direction was determined by calculating the nominal contact pressures for a 20 × 2 mm rectangular contact area that represented the rectangular faced top compression ring. Changes in the contact pressure were achieved by varying the contact area along the stroke length. At a normal contact load of 311 N, dynamic contact pressures over a stroke length of 25 mm were predicted to range from a peak at 62 MPa at the narrowest constriction width of 2.23 mm down to 7.8 MPa when the counter surface was in full contact. The predicted dynamic contact pressures due to the variable geometry as a function of stroke position were shown to closely match the ring radial loads during the four-stroke cycle, Fig. 1. A cylindrical 6 × 20 mm 52100 bearing element (H_v – 755 ± 30) was flat lapped (Kemet 15, 25 μm diamond slurry) on one side to provide the area contact for the reciprocating counter surface. All test surfaces were ultrasonically cleaned in 40–60 Petroleum Ether (Sigma-Aldrich) and dried prior to assembly in the TE77.

2.2. Scuffing methodology

An unformulated synthetic 4 cSt polyalfaolefin (Spectrasyn4, ExxonMobil) was drip fed using a syringe pump at a rate of 0.5 ml/h via a fine bore needle to the low-pressure end of the reciprocating contact to replicate the supply distribution in a fired engine [22,23]. The 52100 rectangular area contact was self-aligned to the cast iron coupon by application of a normal load through a cylindrical pin housed in the counter surface reciprocating clamping head and whose axis was perpendicular to the counter surface. An initial load of 5 N was applied to the contact prior to commencing sliding at 15 Hz whilst observing the contact potential signal to ensure the area contact was not edge loaded. The normal load was then ramped to the test load of 311 N over a period of 300 s followed by a further running in period of 300 s to condition the surfaces at room temperature (RT), Table 1. To induce scuffing, an open loop temperature ramp of 4 °C per minute was initiated by externally heating the lubricant bath, measured by a k-type thermocouple clamped on the specimen surface by the sample fastener at the constricted high pressure end. Two scuffing tests were performed on both a constant flat

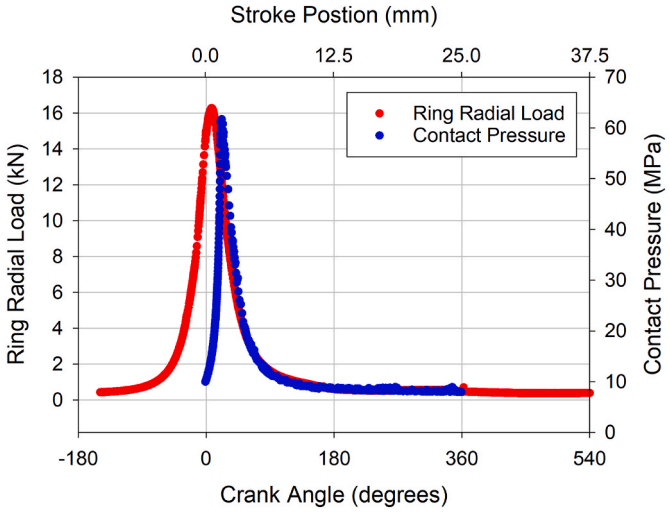

Fig. 1. Radial load profile as a function of crank angle position on the top compression ring of a 12.8-L heavy duty diesel across all four strokes [20].

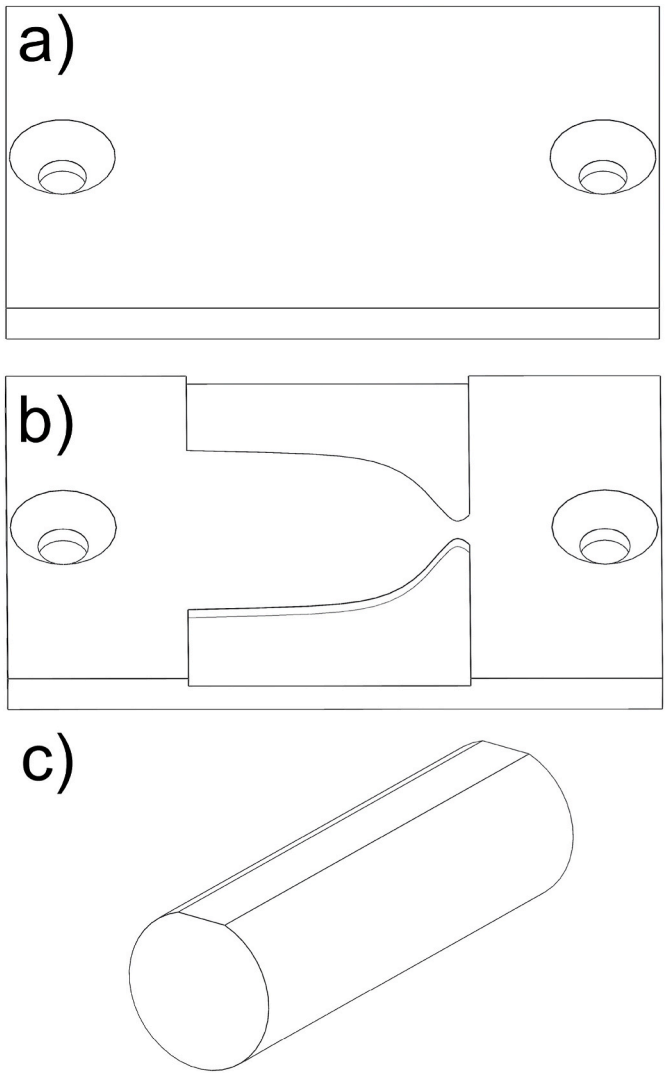

Fig. 2. Schematic images of a) constant pressure, b) dynamic pressure variable geometry cast iron test coupons of dimensions 58 × 38 × 4 mm and c) 6 mm diameter 52100 counter surface with 2 × 20 mm rectangular contact (not to scale).

Table 1
Summary of reciprocating scuffing test conditions.

Normal load (N)	311
Test frequency (Hz)	15
Stroke length (mm)	25
Lubricant	PAO4
Lubricant feed rate (ml/hr)	0.5
RT running-in duration (s)	600
Temperature ramp (°C/min)	4

(unprofiled) and dynamic pressure variable geometry specimens. The constant pressure samples experienced a nominal contact pressure of 7.8 MPa along the entire stroke. Tests were terminated whereupon a rapid increase in the average coefficient of friction indicated severe scuffing. Each test was conducted again on identical samples to ensure the repeatability of the methodology. Test conditions are summarised in Table 1.

2.3. Surface analysis

Upon termination of each test, the surfaces were allowed to cool to room temperature prior to being ultrasonically cleaned again in 40–60 Petroleum Ether. Surface deformation induced by the scuffing process was quantified using a Zeiss optical stereo microscope and an Alicona Infinite Focus focal plane variation microscope (Bruker). Examination of the surface microstructure was conducted using a Zeiss Auriga 60 focused ion beam scanning electron microscope (FIB-SEM) with an Oxford Instruments X-Max detector for energy dispersive x-ray analysis (EDX). Secondary electron images were taken at 5 kV accelerating voltage using a 30 μm aperture and 5 mm working distance. EDX analysis was conducted at an accelerating voltage of 10 kV to ensure appropriate X-ray energy peaks corresponding to the surface composition could be identified, as well as minimising the interaction volume (~300 nm), and a 60 μm aperture to increase the signal strength (counts per second). The morphology of selected subsurface areas was analysed using gallium FIB, at 30 kV:2 nA, where trenches were milled 30 μm in width and 5 μm in depth parallel to the sliding direction, and at 9° from the FIB normal, as it was not possible to physically tilt the specimen to fully perpendicular in the FIB-SEM chamber due to its size. The milled cross-section faces were analysed with secondary electron imaging and EDX.

3. Results

3.1. Coefficient of friction

The recorded signal outputs for the dynamic pressure test 1 are shown in Fig. 3 and were representative for all the scuffing tests performed. Upon initial sliding, formation of a lubricating film was observed by a high contact potential signal of 39.5 mV, however upon commencement of the load ramp to 311 N, the contact potential signal was observed to drop to a minimum value of 0.5 mV, indicating a transition to boundary lubrication. Once the test load of 311 N was achieved, the contact potential signal increased again, indicating recovery of the lubricating film during the running-in phase. Heating of specimen surfaces between 100 and 150 °C again caused a gradual decrease in the contact potential signal such that the boundary lubrication regime was present after 150 °C in all tests.

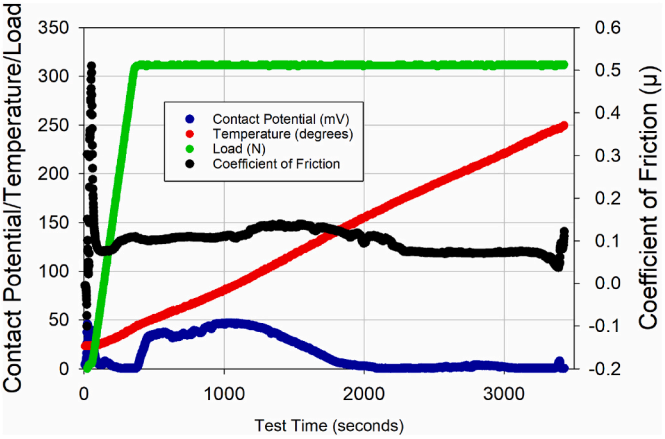

Fig. 3. Test conditions from dynamic pressure test 1 as a function of test time.

Changes in the average coefficient of friction for all tests exhibited poor correlation in terms of absolute individual test time, however, as shown in Fig. 4, there appeared a strong correlation for all tests with test temperature. An increase in the coefficient of friction from preliminary values of around 0.1 was observed for all tests up to approximately 150 °C, concurrent with the transition to boundary lubrication discussed above. The constant pressure samples exhibited a slightly higher average coefficient of friction around a test temperature of 150 °C, but overall the values were very similar for both constant and dynamic pressure specimens. Immediately prior to the onset of severe scuffing, all specimens exhibited low average friction coefficients in the range 0.027–0.077. The temperature of severe scuffing initiation for each test was recorded to be almost identical at 250.8 ± 2.6 °C, as detailed in Table 2.

Stroke resolved friction force and contact potential data from 10 strokes was obtained at 15 kHz trigger frequency immediately prior to initiation (a, c and e) and after scuffing (b, d and f) as shown in Fig. 5. Characteristic resonance from vibration at stroke reversal positions was common to all traces prior to scuffing. For the constant pressure tests, such as those shown in a), there was no observable change in the contact potential signal for friction prior to scuffing. As shown in Fig. 5 b), scuffing for the constant pressure surfaces occurred around the mid-stroke region of the specimen. In contrast, both dynamic pressure tests exhibited a localised increase in the contact potential prior to scuffing, Fig. 5 c) and e). This was accompanied by a concurrent localised decrease in the friction force at these regions, however it was interesting to note that the position of these changes was different for each dynamic pressure test. For the dynamic pressure test 1, these observations were made near the high-pressure area of the sample, whilst for test 2, they were nearer to the mid-stroke position. Upon the transition to scuffing, Fig. 5 d) and f), it appeared that the high friction initiation site was also located within the same region which had moments before exhibited the opposite behaviour.

3.2. Surface analysis

3.2.1. Optical microscopy

Optical macroscope images of all the worn coupon surfaces are shown in Fig. 6. It was observed that rapid adhesive wear (indicated by the white band) occurred at the termination of all tests, with the exception of the constant pressure test 1, Fig. 6 a). It was interesting to note that the adhesive transfer and wear accumulation for the dynamic pressure tests was not necessarily associated with the position of highest

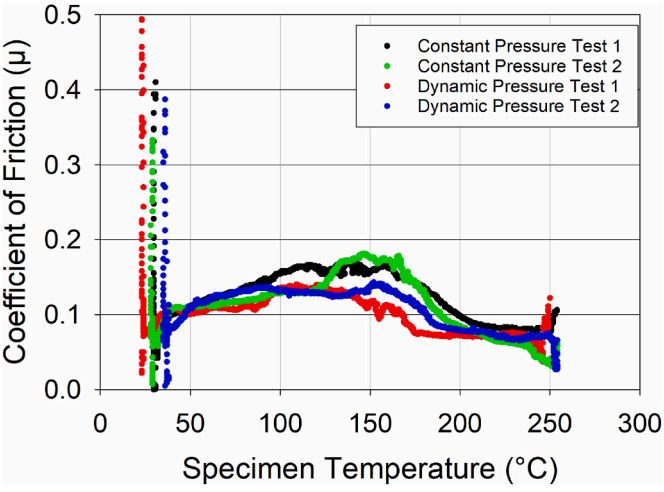

Fig. 4. Average coefficient of friction for scuffing tests plotted again test temperature.

Table 2
Severe scuffing initiation temperatures for constant and dynamic pressure tests.

	Scuffing Temperature (°C)
Constant Pressure Test 1	251
Constant Pressure Test 2	252
Dynamic Pressure Test 1	247
Dynamic Pressure Test 2	253

contact pressure. The influence of contact pressure was observed with respect to the width of the adhesive wear scar, which was constant for the constant pressure test (b) but increased in width for both dynamic pressure tests (c & d) as the contact pressure increased close to the stroke reversal position.

Optical microscopy of a dynamic pressure variable geometry surface before and after scuffing was shown in Fig. 7. The influence of the higher contact pressure at the narrowest position was clearly shown by the change in surface topography. The original grinding marks present on the surface had been entirely removed but only at this specific location. The appearance of surface cracking could be observed across the constriction minima, but was especially apparent around the periphery of the coupon edge.

3.2.2. *Non-contact optical profilometry*

Non-contact optical profilometry with an Alicona Infinite Focus was conducted on both ground and scuffed surfaces as shown in Figs. 8–10.

The average surface roughness (R_a) of the ground cast iron and counter surface specimens was measured to be 1.10 ± 0.24 μm (Figs. 8) and 0.52 ± 0.03 μm, respectively.

For the dynamic pressure variable geometry specimens, the region of the highest contact pressure exhibited significantly more wear compared to the rest of the sliding specimen surface as outline above. Higher magnification optical and corresponding colour depth map images, Fig. 9 a) and b), revealed a much smoother surface compared to the original ground surface, with an average surface roughness R_a of 0.37 ± 0.02 μm.

Despite the decrease in roughness and change in surface morphology within the region of highest contact pressure, the average surface roughness was very similar to that for the low pressure portion of the sample which exhibited a R_a of 0.40 ± 0.07 μm. This region of the sample (away from the adhesive wear scar) was very similar in appearance to the constant pressure specimens, shown in Fig. 10. Wear of the peaks of the ground surface and retention of the original valley resulted in average surface roughness values R_a of 0.36 ± 0.02 μm for the constant pressure surfaces.

All counter surfaces exhibited evidence of good conformal contact with the test coupons with no indication of edge loading. Changes in the contact area due to abrasive wear were minimal and unlikely to affect the contact pressure profile.

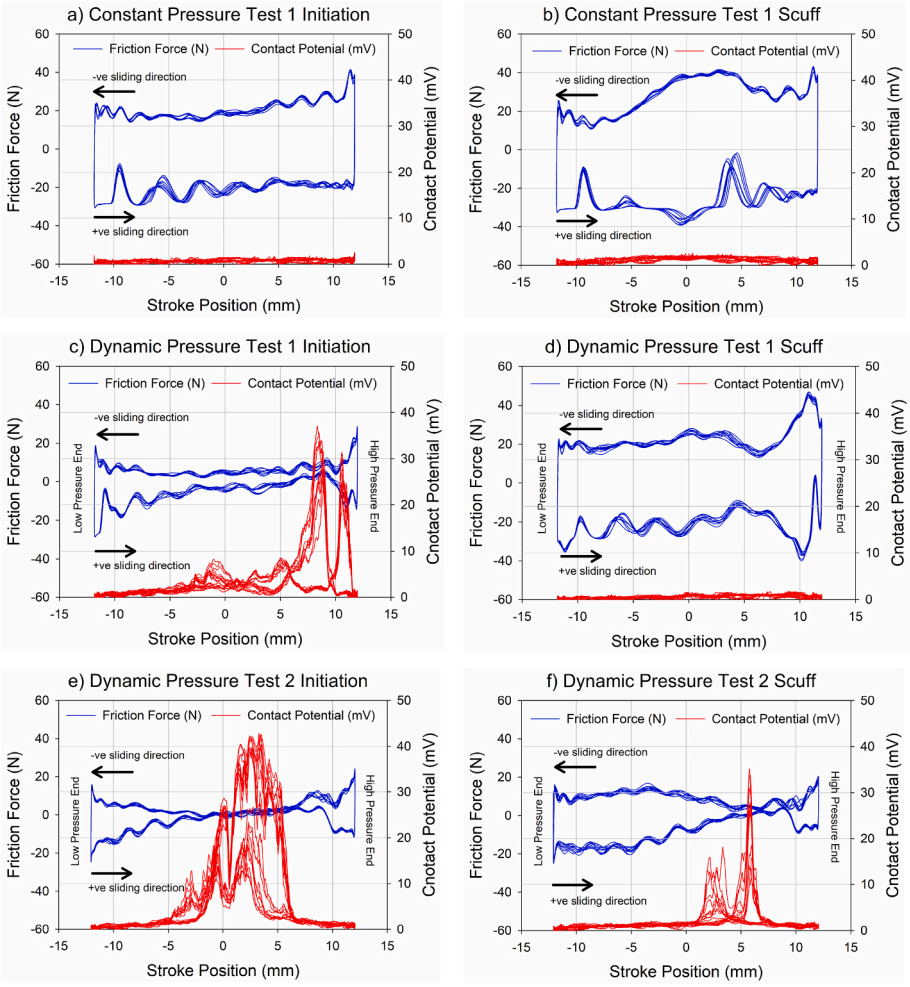

Fig. 5. Stroke resolved friction force and contact potential signals over 10 strokes for constant pressure test 1 (a–b), dynamic pressure test 1 (c–d) and dynamic pressure test 2 (e–f) indicating the onset of initiation and severe scuffing respectively.

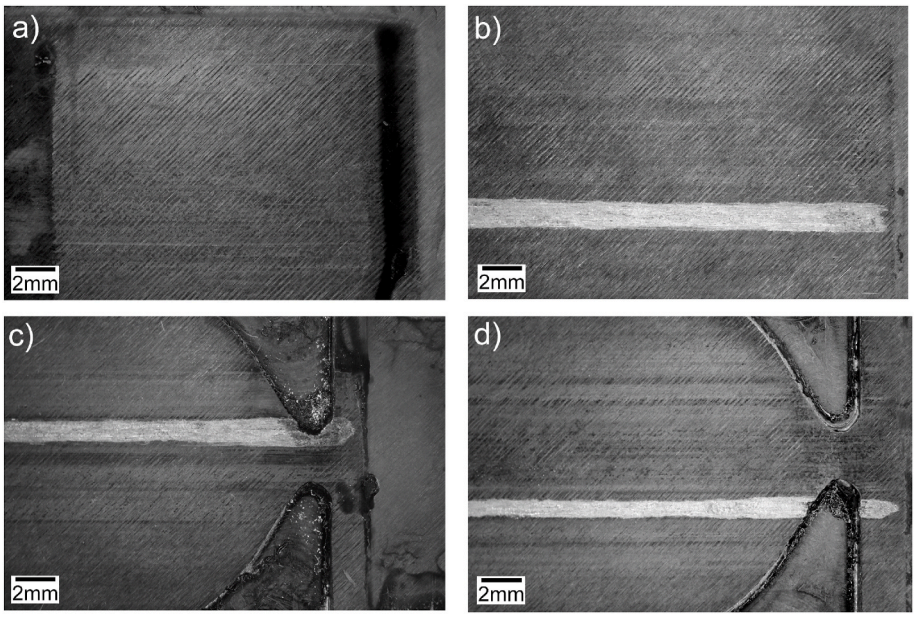

Fig. 6. Optical macroscope images of the constant pressure tests 1(a) and 2(b) and dynamic pressure tests 1 (c) and 2 (d).

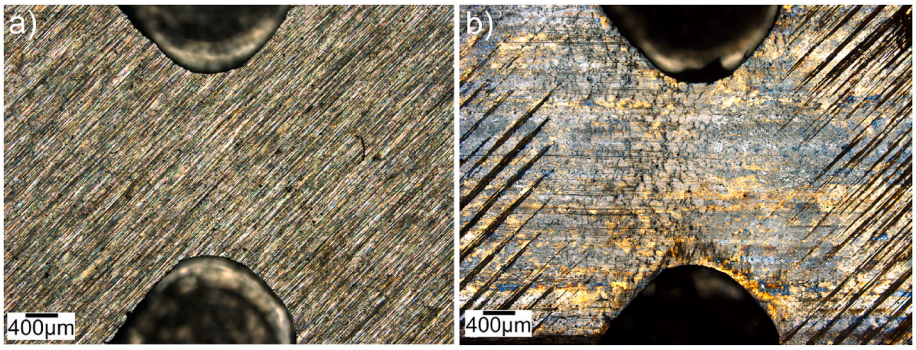

Fig. 7. Optical microscopy images of the high pressure region from dynamic pressure test 2 (a) before and (b) after scuffing test.

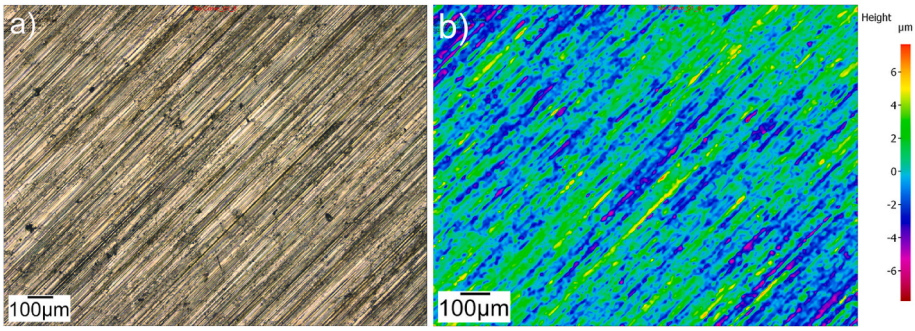

Fig. 8. a) Optical image and b) Colour depth map of the ground flake graphite cast iron surface prior to sliding. (For interpretation of the references to colour in this figure legend, the reader is referred to the Web version of this article.)

3.3. Electron microscopy

A focused ion beam cross section was prepared within the region of the highest contact pressure on the dynamic pressure test 1, Fig. 11, away from the severely scuffed adhesive damage and within the smooth area similar to Fig. 9 a). It was observed that despite the reciprocating nature of the sliding contact, a distinctive strain direction was observed in the sub-surface microstructure, with grains deformed towards the negative stroke position, low pressure direction of the sample. The normalised EDX traces clearly indicated a that oxide layer was present at the sliding interface immediately prior to severe scuffing. The layer appeared to be mostly composed of iron oxide, however it's fragmented appearance was interspersed with regions of carbon and iron presenting variations in signal intensity. The oxide was observed to have filled recesses in the surface suggesting compaction of oxidised wear debris could be a possible mechanism of formation.

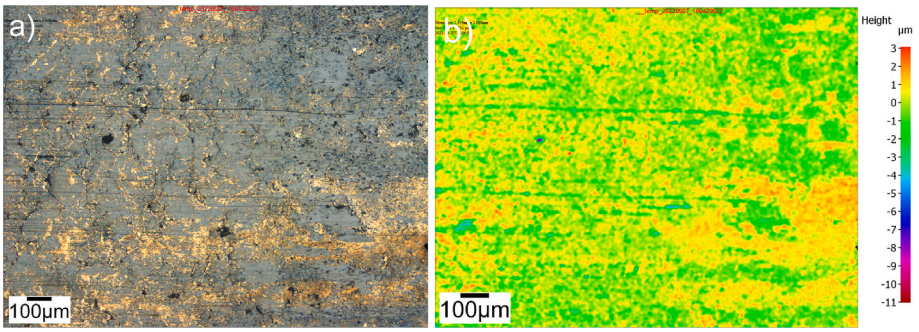

Fig. 9. Optical image (a) and corresponding colour depth map (b) of scuffed dynamic pressure test 2 surface from the region of highest contact pressure. (For interpretation of the references to colour in this figure legend, the reader is referred to the Web version of this article.)

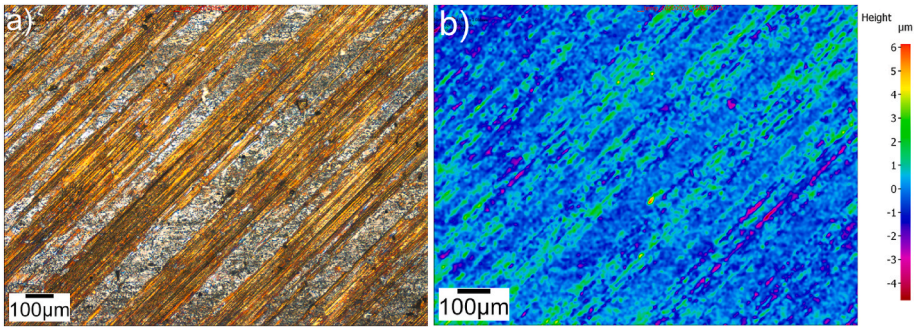

Fig. 10. Optical image (a) and corresponding colour depth map (b) of scuffed constant pressure test 2 surface. (For interpretation of the references to colour in this figure legend, the reader is referred to the Web version of this article.)

4. Discussion

4.1. Influence of dynamic contact pressures

As the width of the counter surface did not significantly change over the course of the experiment, the dynamic contact pressure would have cycled according to that experienced by the top compression ring of a heavy-duty diesel engine. This approach, where counter surface wear is mitigated due to lower contact pressures and a hard material (52100), is advantageous compared to sliding Hertzian line contacts as rapid running-in wear and inconsistent changes to the contact area are avoided, notwithstanding the additional care in alignment required.

The use of a dynamic pressure variable geometry specimen clearly influenced the wear pattern of the cast iron surface as demonstrated in Fig. 7. The removal of the ground lay in this region and the appearance of surface cracks at the narrowest position of the contact, similar to those observed by Kamps et al. [17,18], was strong evidence that a higher contact pressure increased the level of wear during the test compared to the constant pressure specimen. During the latter stages prior to severe scuffing, oxidational wear was the dominant mechanism and damage caused by the higher contact pressure was mitigated by compaction of debris to recesses within the surface. This resulted in similar average surface roughness values for surface regions that experienced both high and low contact pressure despite the clear different in texture observed between Figs. 9 and 10. It was observed in Fig. 6 that once severe scuffing and adhesive transfer to the counter surface had occurred, the influence of a higher contact pressure was to increase the severity of accumulated damage evidenced by the increase in width of the adhesive scar towards the high pressure reversal position.

4.2. Temperature dependence

Despite these observations that variation in the contact pressure influenced the wear patterns, there appeared to be little evidence of a significant influence upon the temperature at which scuffing initiated, as shown in Fig. 4. There was strong evidence that despite an order of magnitude change in nominal contact pressure, the temperature of severe scuffing initiation was always within a couple of degrees as all tests failed at 250.8 ± 2.6 °C. This strongly aligned the results with Blok's critical temperature scuffing theory [24,25], highlighted that scuffing is intrinsically thermal in nature and consistent with similar studies reviewed by Bowman and Stachowiak [6], where desorption initiated around 150 °C before progression to failure between 240 and 250 °C. The influence of a dynamic contact pressure may contribute to surface thermal heating through frictional energy dissipation; however this contribution may have been masked by the heating rate of 4 °C/min, where a lower heating rate may help elucidate this influence in future work. In reality, a heavy-duty diesel engine would not be lubricated by an unformulated fluid, but would have an additive package present to offer some protection from scuffing. This would likely increase the temperature at which initiation occurred, however, given the novelty of this approach it was important to understand the role of the lubricant prior to investigating synergistic effects from chemical additives in future work.

4.3. Oxide formation

Oxidational wear was the dominant wear mechanism prior to severe scuffing as evidenced by the focused ion beam and energy dispersive X-ray analysis shown in Fig. 11. As observed in Figs. 3 and 4, there was a decrease in the average coefficient of friction above approximately 150 °C for all specimens, concurrent with a transition to boundary lubrication conditions as evidenced by the drop in the contact potential signal. It is known that polar molecules in synthetic lubricants such as PAO desorb at around 150 °C [6,26], however such a transition might be expected to result in a higher coefficient of friction. The steady decrease observed was attributed to the onset of mild oxidational wear, similar to that proposed by Stott [27], and caused by elevated flash temperature

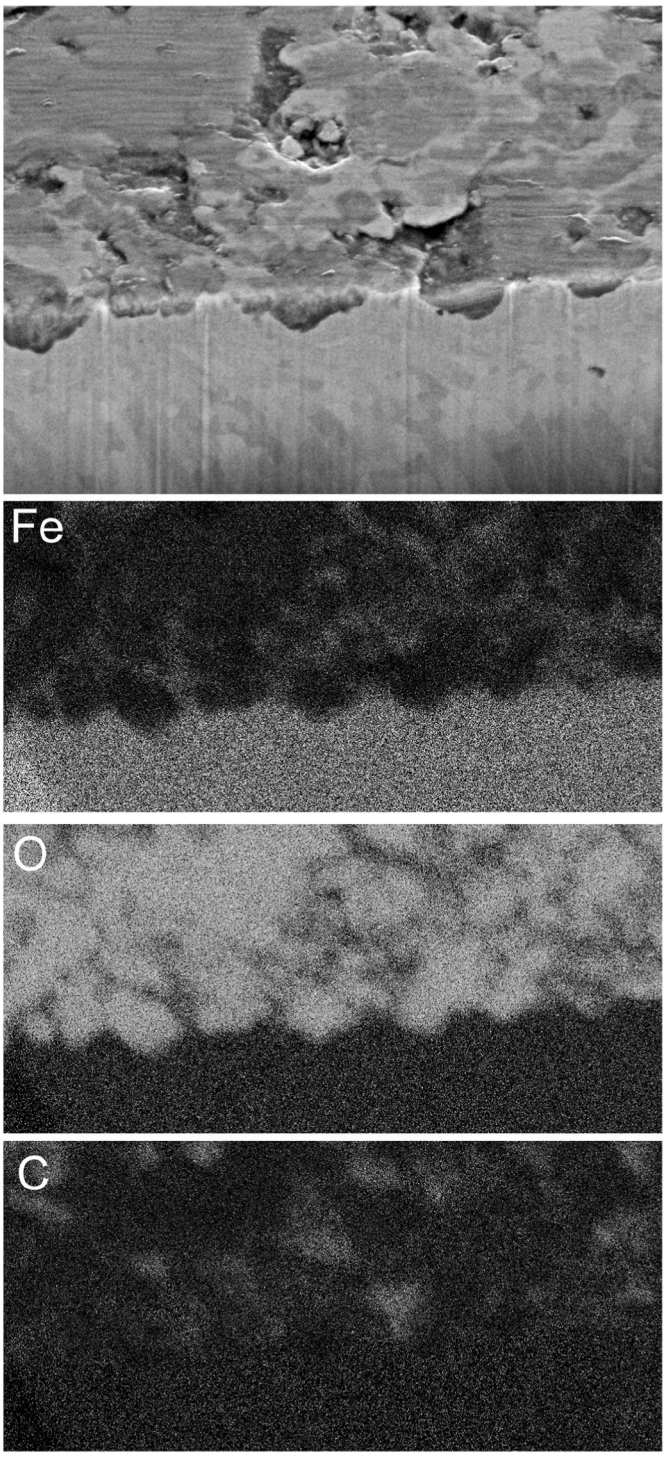

Fig. 11. SEM and EDX images of the FIB cross-section on dynamic pressure test 1: The top image shows a 30 μm wide secondary electron image of both the top surface and FIB cross-section, with the milled edge across the middle of the image. Three EDX element maps of iron, oxygen and carbon are of the same area, where high concentration is shown as white and low concentration as black.

rises from asperity contact at the high points of the ground surface, Fig. 10. Bjerk [28] was one of the early researchers to conclude that surface oxide species could offer protection against scuffing with Quinn highlighting the generic mechanisms of tribological induced oxide formation on ferrous surfaces being determined by the contact temperature [29].

4.4. Scuffing initiation

Immediately prior to severe scuffing initiation, all specimens exhibited a brief transition to a very low friction coefficient between 0.027 and 0.077, shown in Figs. 4 and 5, which does not appear commonly in the literature related to sliding scuffing initiation. For the dynamic pressure specimens, this was concurrent with a peak in the contact potential signal a few seconds before scuffing initiated at the same stroke position, Fig. 5 c) and e) but which was absent for the constant pressure tests. The evidence from the FIB cross-section in Fig. 11 suggested a low friction oxide phase, perhaps similar to a compacted 'glaze' layer [27,30,31] could be responsible for the low average coefficients of friction observed at this stage of the test. Such layers are known to offer low interfacial sliding friction but are transitory, consumptive and not very durable. Whilst Batchelor and Stachowiak [32] suggested that an oxide film 20 Å thick would be sufficient to reduce scuffing of steel surfaces, Rhee and Ludema [33] pointed out interfacial shear strengths of 66 MPa could be expected for tribological induced ferrous oxide films formed on stainless steel. Saeidi et al. [11] found good evidence of the role that different oxide species play in the formation of surface tribo-layers during the scuffing process. Elevated flash temperatures, which have been shown to be as high as 1000 °C with *in situ* XRD scuffing experiments [14–16], could be sufficient to sinter nano-scale oxide debris into a compacted low friction layer, consistent with the image in Fig. 11 which showed an iron oxide compacted into surface recesses. The fact severe scuffing initiation was not exclusive to the region of highest contact pressure on the variable geometry surfaces confirmed that oxide wear debris formation and removal was likely to be the final condition for scuffing initiation, although dynamic contact pressures may have influenced the magnitude of debris generation (Figs. 7 and 9). This was consistent with Ludema [8], Enthoven and Spikes [34], Matsuzaki et al. [4] and Cutiongco and Chung [35] who all pointed out the influence of both temperature as well as transitory wear debris formation and removal on scuffing initiation.

5. Conclusions

The present work has shown it possible to replicate the dynamic contact pressures experienced by a heavy-duty diesel engine on a laboratory scale tribometer using rectangular contact with a variable geometry specimen. Whilst changes in the nominal contact pressure were observed to cause differential wear, initiation of severe scuffing was not influenced by the dynamic pressure profile, but instead was dependent on the surface temperature which was measured to be 250.8 ± 2.6 °C for all tests. Oxidational wear played a significant role in the observed friction behaviour, with compacted wear debris forming a transitory low friction oxide 'glaze' layer which exhibited average coefficients of friction as low as 0.02. Removal of this layer facilitated the initiation of severe scuffing and adhesive wear between surfaces.

Declaration of competing interest

The authors declare that they have no known competing financial interests or personal relationships that could have appeared to influence the work reported in this paper.

Acknowledgements

The authors would like to acknowledge funding from the National Measurement System of the Department for Business, Energy and Industrial Strategy, UK.

References

[1] V. Macián, B. Tormos, V. Bermúdez, L. Ramírez, Assessment of the effect of low viscosity oils usage on a light duty diesel engine fuel consumption in stationary and transient conditions, Tribol. Int. 79 (2014) 132–139.

[2] B. Tormos, L. Ramírez, J. Johansson, M. Björling, R. Larsson, Fuel consumption and friction benefits of low viscosity engine oils for heavy duty applications, Tribol. Int. 110 (2017) 23–34.

[3] C. Zhang, H.S. Cheng, Q.J. Wang, Scuffing behavior of piston-pin/bore bearing in mixed lubrication—Part II: scuffing mechanism and failure criterion, Tribol. Trans. 47 (2004) 149–156.

[4] Y. Matsuzaki, K. Yagi, J. Sugimura, In situ observation of heat generation behaviour on steel surface during scuffing process, Tribol. Lett. 66 (2018) 142.

[5] O. Ajayi, C. Lorenzo-Martin, R. Erck, G. Fenske, Scuffing mechanism of near-surface material during lubricated severe sliding contact, Wear 271 (2011) 1750–1753.

[6] W. Bowman, G. Stachowiak, A review of scuffing models, Tribol. Lett. 2 (1996) 113–131.

[7] O.f.E.C.-o.a. Development, Glossary of Terms and Definitions in the Field of Friction, Wear and Lubrication, OECD, Paris, 1969.

[8] K.C. Ludema, A review of scuffing and running-in of lubricated surfaces, with asperities and oxides in perspective, Wear 100 (1984) 315–331.

[9] J. Han, R. Zhang, O. Ajayi, G. Barber, Q. Zou, L. Guessous, D. Schall, S. Alnabulsi, Scuffing behavior of gray iron and 1080 steel in reciprocating and rotational sliding, Wear 271 (2011) 1854–1861.

[10] Y. Wang, S.C. Tung, Scuffing and wear behavior of aluminum piston skirt coatings against aluminum cylinder bore, Wear 225–229 (1999) 1100–1108.

[11] F. Saeidi, A. Taylor, B. Meylan, P. Hoffmann, K. Wasmer, Origin of scuffing in grey cast iron-steel tribo-system, Mater. Des. 116 (2017) 622–630.

[12] M. Shuster, D. Combs, K. Karrip, D. Burke, Piston ring cylinder liner scuffing phenomenon studies using acoustic emission technique, SAE Trans. (2000) 901–913.

[13] J.E. Booth, T.J. Harvey, R.J.K. Wood, H.E.G. Powrie, Scuffing detection of TU3 cam–follower contacts by electrostatic charge condition monitoring, Tribol. Int. 43 (2010) 113–128.

[14] T. Izumi, K. Yagi, J. Koyamachi, K. Saito, S. Sanda, S. Yamaguchi, H. Ikehata, Y. Yogo, J. Sugimura, Surface deteriorations during scuffing process of steel and analysis of their contribution to wear using in situ synchrotron X-ray diffraction and optical observations, Tribol. Lett. 66 (2018) 120.

[15] S. Kajita, K. Yagi, T. Izumi, J. Koyamachi, M. Tohyama, K. Saito, J. Sugimura, In situ X-ray diffraction study of phase transformation of steel in scuffing process, Tribol. Lett. 57 (2015) 6.

[16] K. Yagi, S. Kajita, T. Izumi, J. Koyamachi, M. Tohyama, K. Saito, J. Sugimura, Simultaneous synchrotron X-ray diffraction, near-infrared, and visible in situ observation of scuffing process of steel in sliding contact, Tribol. Lett. 61 (2016) 19.

[17] T. Kamps, J. Walker, R. Wood, P. Lee, A. Plint, Reproducing automotive engine scuffing using a lubricated reciprocating contact, Wear 332 (2015) 1193–1199.

[18] T. Kamps, J. Walker, R. Wood, P. Lee, A. Plint, Scuffing mechanisms of EN-GJS 400-15 spheroidal graphite cast iron against a 52100 bearing steel in a PAO lubricated reciprocating contact, Wear 376 (2017) 1542–1551.

[19] J. Qu, J.J. Truhan, P.J. Blau, Investigation of the scuffing characteristics of candidate materials for heavy duty diesel fuel injectors, Tribol. Int. 38 (2005) 381–390.

[20] J. Walker, Z. Barnes, A. Abdelbaset, P. Jiang, T. Kamps, Variable pressure scuffing of a flake graphite cast iron diesel cylinder liner, Tribol. Int. 179 (2023), 108155.

[21] M. Priest, C.M. Taylor, Automobile engine tribology — approaching the surface, Wear 241 (2000) 193–203.

[22] T. Seki, K. Nakayama, T. Yamada, A. Yoshida, M. Takiguchi, A study on variation in oil film thickness of a piston ring package: variation of oil film thickness in piston sliding direction, JSAE Rev. 21 (2000) 315–320.

[23] M. Takiguchi, Variation of oil film thickness of piston ring of a internal combustion engine, in: Proceedings of the 14th Internal Combustion Engine Symposium, 1997, pp. 367–373.

[24] H. Blok, The Postulate about the Constancy of Scoring Temperature, 237, NASA Special Publication, 1970, p. 153.

[25] H. Blok, The Surface Temperatures under Extreme Pressure Lubricating Conditions, Laboratorium der Royal Dutch Shell, 1937.

[26] S. Hsu, M. Shen, E. Klaus, H. Cheng, P. Lacey, Mechano-chemical model: reaction temperatures in a concentrated contact, Wear 175 (1994) 209–218.

[27] F.H. Stott, High-temperature sliding wear of metals, Tribol. Int. 35 (2002) 489–495.

[28] R.O. Bjerk, Oxygen—an "extreme-pressure agent", ASLE Transactions 16 (1973) 97–106.

[29] T.F.J. Quinn, Review of oxidational wear: Part I: the origins of oxidational wear, Tribol. Int. 16 (1983) 257–271.

[30] J. Walker, I. Ross, C. Reinhard, W. Rainforth, P.E. Hovsepian, High temperature tribological performance of CrAlYN/CrN nanoscale multilayer coatings deposited on γ-TiAl, Wear 267 (2009) 965–975.

[31] J. Jiang, F. Stott, M. Stack, A generic model for dry sliding wear of metals at elevated temperatures, Wear 256 (2004) 973–985.

[32] A. Batchelor, G. Stachowiak, Some kinetic aspects of extreme pressure lubrication, Wear 108 (1986) 185–199.

[33] S. Rhee, K.C. Ludema, Mechanisms of formation of polymeric transfer films, Wear 46 (1978) 231–240.

[34] J. Enthoven, H.A. Spikes, Infrared and visual study of the mechanisms of scuffing, Tribol. Trans. 39 (1996) 441–447.

[35] E.C. Cutiongco, Y.-W. Chung, Prediction of scuffing failure based on competitive kinetics of oxide formation and removal: application to lubricated sliding of AISI 52100 steel on steel, Tribol. Trans. 37 (1994) 622–628.